JOURNAL OF AIRCRAFT
Vol. 33, No. 4, July–August 1996

Active Control of Panel Flutter with Piezoelectric Transducers

Kenneth D. Frampton,* Robert L. Clark,† and Earl H. Dowell‡
Duke University, Durham, North Carolina 27708-0302

This article investigates the active control of panel flutter with piezoelectric transducers and including linearized potential flow aerodynamics. The aerodynamic modeling is accomplished by approximating the aerodynamic generalized forces with infinite impulse response filters. These filters are coupled to the in vacuo panel dynamic system in feedback, thus, creating a coupled, aeroelastic system. The panel model is developed from a Rayleigh–Ritz approach and includes the mass and stiffness effects of a piezoelectric transducer. Acting as a self-sensing actuator, the piezoelectric transducer is used to implement direct rate feedback control. Results of an analytical implementation of this control system demonstrate a significant increase in the flutter boundaries.

Nomenclature

A, B, F, G = state-space matrices
a = panel length, chord
a_∞ = speed of sound
b = panel width, span
C_p = piezoelectric capacitance matrix
D = $EI/(1-\nu^2)$, stiffness
D_{mn} = aerodynamic influence coefficient
d_{31} = piezoelectric constant
$H_{mn}(t)$ = aerodynamic influence function
h = thickness
$I_{mn}(t)$ = aerodynamic influence function
$\boldsymbol{i}$ = output current vector
K = stiffness matrix
M = Mach number
M_p = structural mass matrix
M_s = piezo mass matrix
N = number of expansion modes
$\hat{P}(z)$ = approximate z-transfer function
$p(x, y, t)$ = aerodynamic pressure
$Q_n(t)$ = generalized force
$q_n(t)$ = generalized coordinate
$r_n(s)$ = $q_n(s)/h_s$
S_{mn} = aerodynamic influence coefficient
S_p = piezo area moment of inertia
s = tU_a/a
t = time
U_a = freestream velocity
$\boldsymbol{u}$ = state-space input vector
$\hat{v}$ = $v_n/v_{\max}$
$v_{\max}$ = piezo saturation voltage
v_n = input voltage
$w(x, y, t)$ = panel displacement
x, y, z = Cartesian coordinates
$\boldsymbol{x}$ = state vector
$\boldsymbol{y}$ = output vector
α, γ = Fourier transform variables
ε = $d_{31}v_{\max}a^2E_pS_p/D_ph_s(1-\nu_p)$
Θ = electromechanical coupling matrix
λ = $\rho_aU_a^2a^3/D$
μ_a = ρ_aa/ρ_sh_s
μ_p = ρ_ph_p/ρ_sh_s
ρ = density
σ = D_p/D_s
τ = integration dummy variable
$\phi(x, y, z, t)$ = fluid velocity potential
$\Psi_n(x, y)$ = modal expansion functions

Subscripts
a = aerodynamic
m, n = modal indices
p = piezoelectric
s = structural

Introduction

THE recent emergence of technology capable of performing the necessary computational and actuation tasks has led to the application of active control to many problems in dynamics. However, while much attention has been focused in the literature on active control of wing flutter, very little has been done in the area of panel flutter control. The phenomena of panel flutter has been studied for many years, but the few available references that apply active control to panel flutter use piston theory or quasisteady aerodynamics as the working model.[1,2] The use of piston theory is not without good reason since it is reasonably accurate at higher Mach numbers and modeling the effects of linearized potential flow (which is necessary for Mach numbers below 1.5), in a state-space representation suitable for control investigations is difficult. However, it is the transonic and low supersonic range that is usually most critical for flutter. For this reason, the inclusion of full potential flow aerodynamics is important to effective control system design.

This article investigates the active control of panel flutter including linearized potential flow aerodynamics. Development of the aeroelectroelastic model consists of combining the electroelastic panel model developed by Hagood et al.[3] with the aeroelastic panel model introduced by Frampton et al.[4] The electroelastic panel model combines the dynamics of a plate with the dynamics of piezoelectric transducers through a Rayleigh–Ritz formulation. The aeroelastic panel model is created by coupling a set of aerodynamic force approximating filters in feedback with an in vacuo panel model. The set of filters is constructed from the aerodynamic influence functions as developed by Dowell,[5,6] using Prony's method.

The control scheme used in this investigation is direct rate feedback (DRFB). This is implemented by using a piezoelec-

Received May 21, 1995; revision received Jan. 24, 1996; accepted for publication Feb. 12, 1996.

*Graduate Research Assistant, Department of Mechanical Engineering and Materials Science. Student Member AIAA.

†Assistant Professor, Department of Mechanical Engineering and Materials Science. Member AIAA.

‡J. A. Jones Professor and Dean, School of Engineering, Department of Mechanical Engineering and Materials Science. Fellow AIAA.

tric transducer simultaneously as a sensor and actuator as described by Anderson et al.,[7] Dosch and Inman,[8] and more recently Cole and Clark.[9] The piezoelectric transducer sensor signal, which is proportional to the strain rate, is amplified and fed back to itself as a control signal.

The effectiveness of this control system in delaying the onset of flutter is presented. In addition, the importance of considering full potential flow aerodynamics in a control system design is demonstrated. Also, the effect of piezoelectric transducer saturation is addressed.

Aeroelectroelasticity

Panel and Piezoelectric Transducer Dynamics

The panel in this investigation combines the aeroelastic modeling introduced by Frampton et al.[4] with the electroelastic modeling described by Hagood et al.[3] This method employs a Rayleigh–Ritz formulation to discretize the coupled equations of motion for the piezoelectric sensor/actuator and the aeroelastic panel. The combination of the two, which includes the mass and stiffness effects of the panel and the piezoelectric transducer, is referred to as an aeroelastic piezostructure.

This method assumes a separable solution using the in vacuo panel eigenfunctions and generalized coordinates of the form

$$w(x, y, t) = \sum_{n=1}^{N} \Psi_n(x, y) q_n(t) \tag{1}$$

and a linear voltage distribution across the piezoelectric thickness. The resulting actuation equations of motion with no structural damping are

$$[M_s + M_p]\{\ddot{q}\} + [K_s + K_p]\{q\} = [\Theta]\{v\} - \rho_a U_a^2 \{Q\} \tag{2}$$

and the rate sensor equations are

$$[\Theta]^T\{\dot{q}\} + [C_p]\{\dot{v}\} = \{i\} \tag{3}$$

where

$$\{q\} = \{q_1 \quad q_2 \quad \cdots \quad q_n\}^T \tag{4}$$

$$\{Q\} = \{Q_1 \quad Q_2 \quad \cdots \quad Q_n\}^T \tag{5}$$

$$\{v\} = \{v_1 \quad v_2 \quad \cdots \quad v_n\}^T \tag{6}$$

The aerodynamic generalized forces Q_n are a function of the aerodynamic pressure

$$Q_n(t) = \int_0^b \int_0^a \frac{p(x, y, t)}{\rho_a U_a^2} \Psi_n(x, y)\, dx\, dy \tag{7}$$

Definitions of the previous matrices can be found in Ref. 3. The coordinate system for the panel is shown in Fig. 1.

Full Potential Flow Generalized Forces

Consider the case of a simply supported panel with the following eigenfunctions (only one mode in the y direction is used for simplicity):

$$\Psi_n(x, y) = \sin[(n\pi/a)x]\sin[(\pi/b)y] \tag{8}$$

In this case the panel equation of motion [Eq. (2)] can be expressed nondimensionally as

$$[\hat{M}_s + 4\mu_p \hat{M}_p]\{\ddot{r}\} + \left[\frac{\mu_a}{\lambda}\hat{K}_s + 4\frac{\mu_a \sigma}{\lambda}\hat{K}_p\right]\{r\} = 8\frac{\mu_a \sigma \varepsilon}{\lambda}[\hat{\Theta}]\{\hat{v}\} - 4\mu_a\{\hat{Q}\} \tag{9}$$

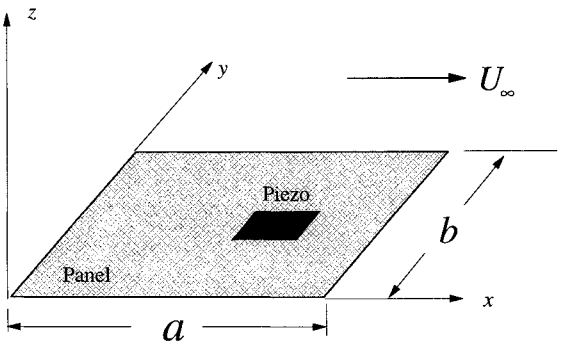

Fig. 1 Panel coordinate system.

where the hat [^], indicates that all dimensional terms have been pulled out of the matrix and included in the nondimensional coefficients.

The generalized forces $Q_n(t)$ are found by solving the partial differential equation describing the velocity potential in an inviscid, irrotational fluid moving parallel to the x axis

$$\nabla^2\phi - \frac{1}{a_\infty^2}\left[\frac{\partial^2\phi}{\partial t^2} + 2U_a\frac{\partial^2\phi}{\partial x \partial t} + U_a^2\frac{\partial^2\phi}{\partial x^2}\right] = 0 \tag{10}$$

subject to the boundary conditions for a panel embedded in an infinite baffle

$$\left.\frac{\partial\phi}{\partial z}\right|_{z=0} = \begin{cases} \dfrac{\partial w}{\partial t} + U_a\dfrac{\partial w}{\partial x} & \text{on the panel} \\ 0 & \text{off the panel} \end{cases} \tag{11}$$

and a finiteness or radiation condition as z approaches infinity.

The solution can be obtained by taking a Laplace transform with respect to time and a double Fourier transform with respect to the x and y spatial coordinates. The transformation is applied to Eqs. (10), (11), and Bernoulli's equation:

$$p = -\rho_a\left[\frac{\partial\phi}{\partial t} + U_a\frac{\partial\phi}{\partial x}\right] \tag{12}$$

while incorporating Eq. (1). Details of the solution process can be found in Refs. 5 and 6.

The solution yields the generalized aerodynamic forces on the panel that are given here as

$$Q_n(t) = \sum_{m=1}^{N} Q_{mn} \tag{13a}$$

where

$$Q_{mn}(t) = q_m(t)S_{mn} + \dot{q}_m(t)D_{mn} + \int_0^t q_m(\tau)H_{mn}(t-\tau)\, d\tau + \int_0^t \dot{q}_m(\tau)I_{mn}(t-\tau)\, d\tau \tag{13b}$$

$$S_{mn} = \frac{1}{M}\int_0^a \int_0^b \frac{\partial\Psi_m}{\partial x}\Psi_n\, dy\, dx \tag{13c}$$

$$D_{mn} = \frac{1}{MU_a}\int_0^a \int_0^b \Psi_m\Psi_n\, dy\, dx \tag{13d}$$

$$H_{mn}(t) = -\frac{U_a}{4\pi^2 M^2}\int_{-\infty}^{\infty}\int_{-\infty}^{\infty} G_{mn} i\alpha\sqrt{\alpha^2+\gamma^2}\,e^{-i\alpha U_a t} \times J_1[a_\infty t\sqrt{\alpha^2+\gamma^2}]\,d\alpha\,d\gamma \tag{13e}$$

$$I_{mn}(t) = -\frac{1}{4\pi^2 M^2}\int_{-\infty}^{\infty}\int_{-\infty}^{\infty} G_{mn}\sqrt{\alpha^2+\gamma^2}\,e^{-i\alpha U_a t} \times J_1[a_\infty t\sqrt{\alpha^2+\gamma^2}]\,d\alpha\,d\gamma \tag{13f}$$

$$G_{mn} = \int_0^a\int_0^b \Psi_m(x,y)e^{-i(\alpha x+\gamma y)}\,dy\,dx \times \int_0^a\int_0^b \Psi_n(x,y)e^{i(\alpha x+\gamma y)}\,dy\,dx \tag{13g}$$

The integrals in Eqs. (13c), (13d), and (13g) can be performed analytically for most panel eigenfunctions. Equations (13e) and (13f), which define the aerodynamic influence functions, must be evaluated numerically.

Piston Theory Generalized Forces

Piston theory is presented here for comparison with the full potential flow solution developed previously. Piston theory assumes that the pressure acting on the panel is equivalent to the pressure acting on a piston in a tube:

$$p = \rho_a a_\infty\left[\frac{\partial w}{\partial t} + U_a\frac{\partial w}{\partial x}\right] \tag{14}$$

The total piston velocity includes a convection term $U_a(\partial w/\partial x)$, as well as a direct velocity term $\partial w/\partial t$. Here the plate is the equivalent piston and the tube is perpendicular to the plate.

Combining Eqs. (1) and (14) and inserting into Eq. (7) yields the piston theory generalized aerodynamic forces

$$Q_n(t) = \sum_{m=1}^{N} Q_{mn} \tag{15a}$$

where

$$Q_{mn}(t) = q_m(t)S_{mn} + \dot{q}_m(t)D_{mn} \tag{15b}$$

$$S_{mn} = \frac{1}{M}\int_0^a\int_0^b \frac{\partial\Psi_m}{\partial x}\Psi_n\,dy\,dx \tag{15c}$$

$$D_{mn} = \frac{1}{MU_a}\int_0^a\int_0^b \Psi_m\Psi_n\,dy\,dx \tag{15d}$$

Note that this result is identical to that obtained from full potential flow analysis if the influence functions [$H_{mn}(t)$ and $I_{mn}(t)$] are ignored.

Approximate Generalized Forces

Since the generalized aerodynamic forces represented in Eq. (13b) are a function of the panel generalized coordinates, they can be viewed as dynamic feedback on the panel. These feedback dynamics are characterized by the influence functions $H_{mn}(t)$ and $I_{mn}(t)$, which represent aerodynamic impulse responses, and the influence coefficients S_{mn} and D_{mn}, which are instantaneous or feed-through dynamics.

Since there is no closed-form solution for the generalized forces some approximation must be made. The approach suggested here is to construct digital filters that approximate these dynamics. A reduced order recursive filter may be constructed by applying Prony's method to the aerodynamic influence functions.[10,11] Prony's method approximates an impulse response (in this case the influence functions) with a set of exponential functions in a least-squares sense. These exponential

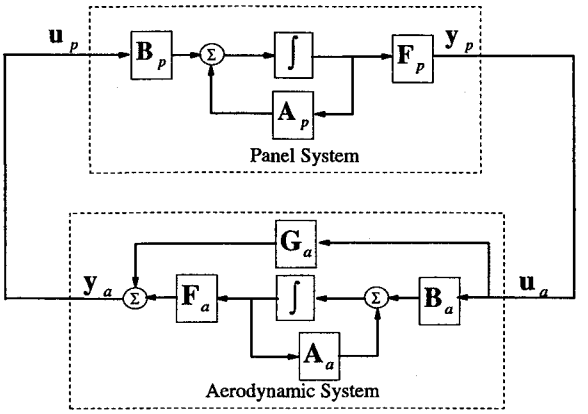

Fig. 2 State-space schematic of the complete aeroelastic system.

approximations to the influence functions can be readily transformed into an lth order infinite impulse response (IIR) filter of the form

$$\hat{P}_{mn}(z) = \sum_{i=0}^{l-1} a_i z^{-i} \Big/ \sum_{i=0}^{l-1} b_i z^{-i} \tag{16}$$

As an example, suppose the values of the influence function $H_{mn}(iT)$ are used to solve for the filter coefficients in Eq. (16). When provided with an input signal that represents the panel generalized coordinate $q_m(iT)$, this filter would output an approximate convolution of $q_m(iT)$ with $H_{mn}(iT)$. Similarly, a filter could be constructed from $I_{mn}(iT)$ and provided with a signal representing $\dot{q}_m(iT)$. Summing the outputs of the two filters would yield an approximation to the dynamic portion of Eq. (13b). Details of this process may be found in Ref. 4.

An approximate filter can be found, as shown previously, for each aerodynamic influence function $H_{mn}(t)$ and $I_{mn}(t)$. A complete set of these filters can then be summed according to Eqs. (13a) and (13b). This would yield a dynamic system that has the generalized coordinates $q_m(t)$ and $\dot{q}_m(t)$ as the inputs and the generalized aerodynamic forces $Q_n(t)$ as the outputs. This system is then coupled as feedback on the panel resulting in a complete aeroelastic system. This is shown schematically (in state-space notation) in Fig. 2.

State-Space Formulation

The actuation equations of motion for the panel described in Eq. (2) can be expressed in state variable form as

$$\dot{x}_s = A_s x_s + B_s u_s \tag{17a}$$

$$y_s = F_s x_s \tag{17b}$$

where

$$x_s = \begin{Bmatrix} q \\ \dot{q} \end{Bmatrix}, \quad u_s = \begin{Bmatrix} Q(t) \\ v_p(t) \end{Bmatrix}, \quad y = \begin{Bmatrix} q \\ \dot{q} \\ i(t) \end{Bmatrix} \tag{17c}$$

$$A_s = \begin{bmatrix} 0 & I \\ -[M_s + M_p]^{-1}[K_s + K_p] & 0 \end{bmatrix} \tag{17d}$$

$$B_s = \begin{bmatrix} 0 & 0 \\ \rho_a U_a^2[M_s + M_p]^{-1} & [M_s + M_p]^{-1}\Theta \end{bmatrix} \tag{17e}$$

$$F_s = \begin{bmatrix} I \\ \Theta^T \end{bmatrix} \tag{17f}$$

The approximate filters of Eq. (16) can be converted to state-space form.[12] Each approximate filter associated with the influence function $H_{mn}(t)$ and $I_{mn}(t)$ has a state-space representation with matrices $\{A_{H_{mn}}, B_{H_{mn}}, F_{H_{mn}}, G_{H_{mn}}\}$ and $\{A_{I_{mn}}, A_{I_{mn}}, F_{I_{mn}}, G_{I_{mn}}\}$, respectively. The complete set of state-space repre-

sentations can be assembled to form the approximate aerodynamic system as follows:

$$\boldsymbol{x}_a = A_a \boldsymbol{x}_a + B_a \boldsymbol{u}_a \tag{18a}$$

$$\boldsymbol{y}_a = F_a \boldsymbol{x}_a + G_a \boldsymbol{u}_a \tag{18b}$$

where

$$\boldsymbol{y}_a = \{Q_1(t) \quad Q_2(t) \quad \cdots \quad Q_n(t)\}^T \tag{18c}$$

$$\boldsymbol{u}_a = \{q_1 \quad \dot{q}_1 \quad q_2 \quad \dot{q}_2 \quad \cdots \quad q_n \quad \dot{q}_n\}^T \tag{18d}$$

$$A_a = \begin{bmatrix} A_{H_{11}} & 0 & \cdots & 0 & 0 \\ 0 & A_{I_{11}} & \cdots & 0 & 0 \\ \vdots & \vdots & \ddots & \vdots & \vdots \\ 0 & 0 & \cdots & A_{H_{mn}} & 0 \\ 0 & 0 & \cdots & 0 & A_{I_{mn}} \end{bmatrix} \tag{18e}$$

$$B_a = \begin{bmatrix} B_{H_{11}} & 0 & \cdots & 0 & 0 \\ 0 & B_{I_{11}} & \cdots & 0 & 0 \\ \vdots & \vdots & \ddots & \vdots & \vdots \\ 0 & 0 & \cdots & B_{H_{1n}} & 0 \\ 0 & 0 & \cdots & 0 & B_{I_{1n}} \\ \vdots & \vdots & \vdots & \vdots & \vdots \\ B_{H_{m1}} & 0 & \cdots & 0 & 0 \\ 0 & B_{I_{m1}} & \cdots & 0 & 0 \\ \vdots & \vdots & \ddots & \vdots & \vdots \\ 0 & 0 & \cdots & B_{H_{mn}} & 0 \\ 0 & 0 & \cdots & 0 & B_{I_{mn}} \end{bmatrix} \tag{18f}$$

$$F_a = \begin{bmatrix} F_{H_{11}} & F_{I_{11}} & \cdots & F_{H_{1n}} & F_{I_{1n}} \\ F_{H_{21}} & F_{I_{21}} & \cdots & F_{H_{2n}} & F_{I_{2n}} \\ \vdots & \vdots & \ddots & \vdots & \vdots \\ F_{H_{m1}} & F_{I_{m1}} & \cdots & F_{H_{mn}} & F_{I_{mn}} \end{bmatrix} \tag{18g}$$

$$G_a = \begin{bmatrix} G'_{H_{11}} & G'_{I_{11}} & \cdots & G'_{H_{1n}} & G'_{I_{1n}} \\ G'_{H_{21}} & G'_{I_{21}} & \cdots & G'_{H_{2n}} & G'_{I_{2n}} \\ \vdots & \vdots & \ddots & \vdots & \vdots \\ G'_{H_{m1}} & G'_{I_{m1}} & \cdots & G'_{H_{mn}} & G'_{I_{mn}} \end{bmatrix} \tag{18h}$$

and the influence coefficients are incorporated as follows:

$$G'_{H_{mn}} = G_{H_{mn}} + S_{mn} \tag{18i}$$

$$G'_{I_{mn}} = G_{I_{mn}} + D_{mn} \tag{18j}$$

The aerodynamic states $\boldsymbol{x}_a$ are of mathematical construct and have no physical significance. The panel and aerodynamic state-space models can then be coupled together as shown in Fig. 2.

The accuracy of this model can be demonstrated by comparing the flutter boundaries with those reported in the literature.[5,6,13,14] The flutter boundaries are determined by increasing the nondimensional dynamic pressure λ while holding all other parameters fixed. Flutter occurs when one of the system eigenvalues moves into the right-half-plane.

A comparison of flutter dynamic pressure vs Mach number is shown in Fig. 3. Results are illustrated for a panel with mass ratios of $\mu_a = 0.1$ and $\mu_p = 0.5$, $\sigma = 1.2$, $\varepsilon = 130$, and dimension ratio $a/b = 1$, using a four-mode panel model. The figure shows the flutter boundaries for the plate with and without a piezoelectric transducer for both full potential flow and piston theory aerodynamics. Note that the presence of the piezoelectric transducer slightly increases the flutter boundary. This is because of the increased panel mass with the transducer. Also note that the two aerodynamic theories approach each other asymptotically as the Mach number increases. However, for Mach numbers below 1.5 the theory incorporating linearized potential flow aerodynamics predicts flutter boundaries well

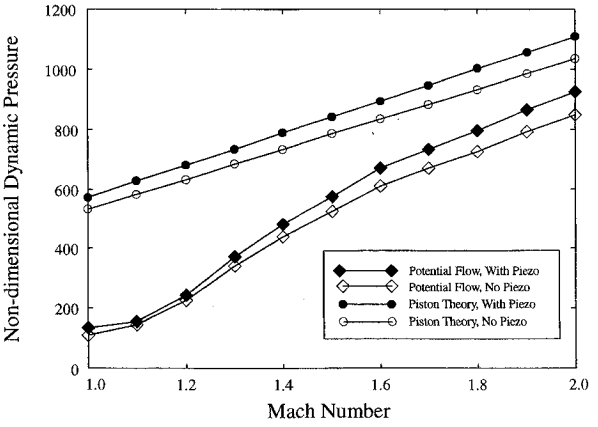

Fig. 3 λ_f vs M for a panel aspect ratio of $a/b = 1$.

below that predicted by piston theory. These results are consistent with those obtained by Dowell.[5,6] A more detailed discussion of the model validity can be found in Ref. 4.

Collocated Direct Rate Feedback Control

Collocated direct rate feedback control is a well-documented form of control which, in the absence of sensor/actuator dynamics and rigid body modes, has guaranteed stability for any positive feedback gain.[15]

Collocation is achieved by using a piezoceramic transduction device as a sensoriactuator,[9] i.e., simultaneously as a sensor and actuator.[7-9,16] By applying the appropriate circuitry to the piezoelectric transducer, the portion of the piezoelectric output that is proportional to the structural velocity can be isolated. This is equivalent to rendering Eq. (3) as

$$[\Theta]^T\{\dot{q}\} = \{i\} \tag{19}$$

Direct rate feedback control consists of feeding back a signal proportional to the sensor current i from Eq. (19) as the voltage input v to Eq. (2).

Results

The effectiveness of collocated direct rate feedback control is demonstrated by applying the control to the aeroelastic panel model and finding the flutter instability boundaries. All results in this section are for the following parameters: $\mu_p = 0.5$, $\mu_a = 0.1$, $\sigma = 1.2$, $\varepsilon = 130$, and $a/b = 1.0$. These parameters correspond to typical values for G-1195-type piezoceramic and a steel panel. Previous investigations have shown that mass ratio has relatively little effect on the flutter boundaries,[14] therefore, the mass ratios μ_p and μ_a are held constant.

Selection of the piezoelectric transducer location is very important for a successful control system design. Formal optimization of transducer location was not performed, however, investigation into the aeroelastic mode shapes suggests a good location. It is well known that piezoelectric transducers are most effective when located in regions of high strain (i.e., high panel curvature). Since the goal is to control flutter, the flutter mode shapes must be considered when looking for advantageous locations. This approach was also considered by Scott and Weisshaar.[1]

The normalized flutter mode shapes in the chordwise direction are shown in Fig. 4 for various Mach numbers. Note the strong influence of the 1st and 2nd in vacuo modes on the flutter mode. The region of maximum strain at each Mach number occurs very near $x/a = 0.7$. For this reason a transducer coverage of $0.6 < x/a < 0.8$ and $0.4 < y/b < 0.6$ was selected. This chordwise location also corresponds to the maximum delay in the migration of open loop zeros into the right-half-plane. The importance of the zero migration delay will be discussed in more detail later.

Results from this analysis are shown in Fig. 5 for the full potential flow model and several feedback gains. Figure 5 demonstrates that, except near $M = 1.0$, the use of direct rate feedback control is equally effective at all Mach numbers in terms of a percentage increase in flutter dynamic pressure. Note in Fig. 5 that there is a maximum flutter boundary that direct rate feedback can achieve. This is demonstrated by the coincidence of the flutter boundary for feedback gains of 0.1 and 0.2.

This behavior is better illustrated in Fig. 6, which shows the change in flutter nondimensional dynamic pressure with increasing feedback gain for three Mach numbers. Also included in Fig. 6 are similar results for a piston theory aerodynamic model. It is apparent in Fig. 6 that the piston theory model overpredicts the control effectiveness, particularly at lower Mach numbers, compared to the full potential flow model. Also note that the difference between the full potential flow model and the piston theory model increases with increasing gain.

An important result demonstrated in Fig. 6 is that, at a fixed Mach number, there is a maximum flutter dynamic pressure that direct rate feedback control can achieve. This is evident in the asymptotic behavior of the flutter boundaries with increasing gain shown in Fig. 6. In other words, for a fixed Mach number, there is a limiting nondimensional dynamic pressure λ, beyond which direct rate feedback control cannot stabilize the system.

This limitation is because of the mechanism by which direct rate feedback control stabilizes the system. Stabilization is accomplished by moving the open-loop poles toward the open-loop zeros. This is demonstrated in Fig. 7, which shows the closed-loop root locus for a four-mode panel (aerodynamic poles are omitted for clarity). Results in Fig. 7 are for a Mach number of 2.0 and dynamic pressure $\lambda = 1300$, which is greater than the open-loop flutter dynamic pressure, but less than the limiting dynamic pressure. Note in Fig. 7 that as the feedback gain is increased the unstable poles are drawn toward the open-loop zeros that are located in the left-half-plane. Therefore, given enough feedback gain, the system can be stabilized.

Unfortunately, it is not always the case that the open-loop zeros, toward which the unstable poles are drawn, lie in the left-half-plane. The location of these open-loop zeros is a function of M, mass ratio μ_a, the sensoriactuator location, and most strongly a function of the dynamic pressure λ. This dependence is demonstrated in Fig. 8, which shows the locus of the system zeros as a function of λ. This plot is for a Mach number of 2.0. Note the migration path of the zeros. At a dynamic pressure of $\lambda = 1593$, a pair of zeros moves into the right-half-plane. Piston theory predicts that the zero will move into the right-half-plane at a dynamic pressure of $\lambda = 1903$. This accounts for the large difference in maximum flutter dynamic pressure depicted in Fig. 6.

A root locus similar to that in Fig. 7, but with $\lambda = 1630$, is shown in Fig. 9. Note how the pair of unstable poles is moved toward a pair of zeros in the right-half-plane. Therefore, no amount of feedback gain could stabilize the system. The point at which the open-loop zeros moves into the right-half-plane is the closed-loop flutter boundary. Beyond this point, even with direct rate feedback control, the panel will flutter.

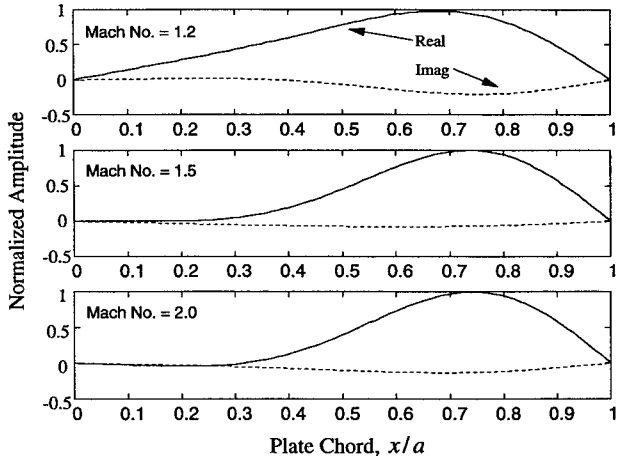

Fig. 4 Flutter mode shapes for various Mach numbers.

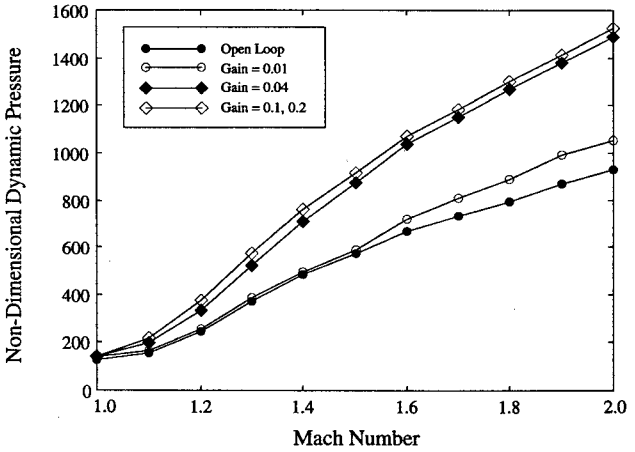

Fig. 5 λ_f vs M for various feedback gains.

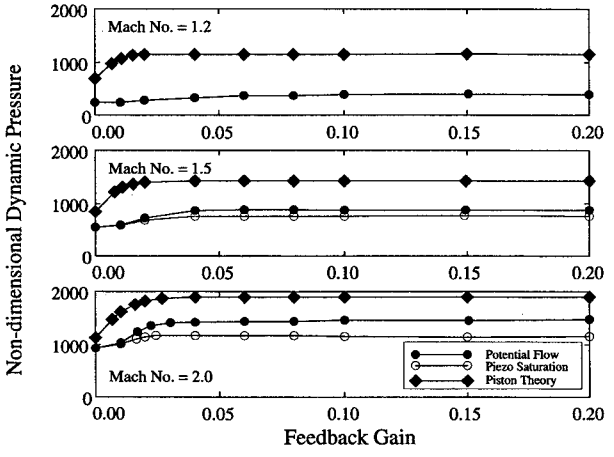

Fig. 6 Flutter boundaries with varying feedback gain.

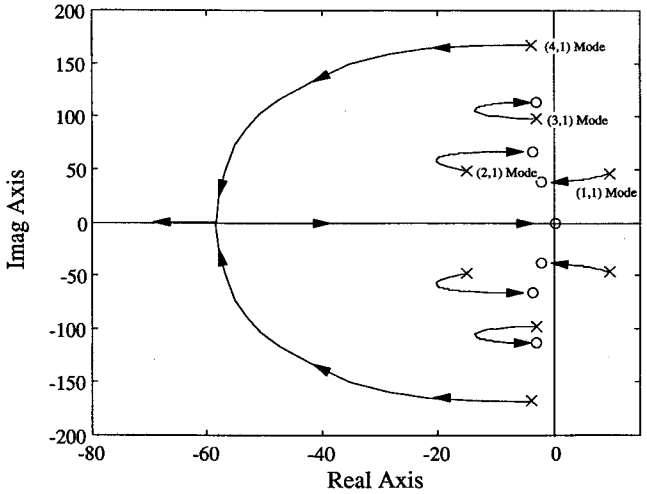

Fig. 7 Root locus of the full potential flow model ($\lambda = 1300$) with feedback gain varying from 0 (corresponding to the open-loop pole, x) to ∞ (corresponding to the open-loop zero, ○).

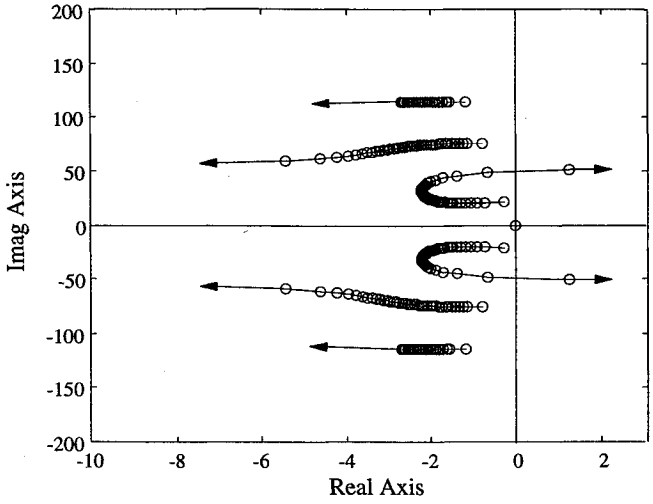

Fig. 8 Zero locus of the full potential flow model with nondimensional dynamic pressure varying from $\lambda = 0$ to $\lambda = 1600$ (○ = zero).

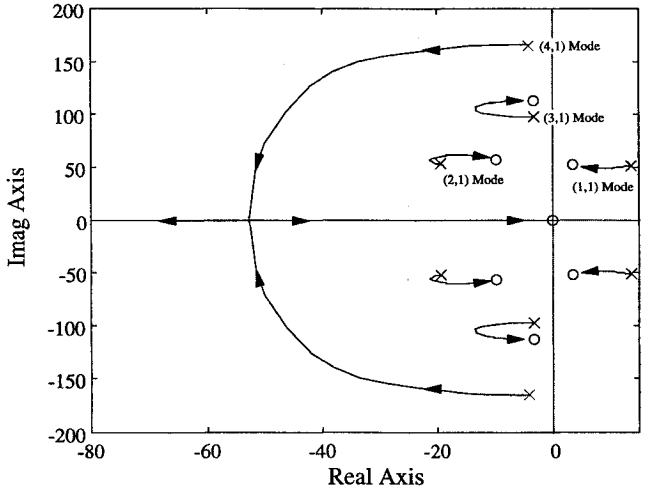

Fig. 9 Root locus of the full potential flow model ($\lambda = 1630$) with feedback gain varying from 0 (corresponding to the open-loop pole, ×) to ∞ (corresponding to the open-loop zero, ○).

Although this demonstrates a limit to the amount that direct rate feedback control can increase the flutter boundary, other feedback control techniques could potentially increase the boundary further. Since the migration of the open-loop zeros is, in part, a function of the location of the sensoriactuator, its size and location on the aeroelastic panel could be formally optimized to further delay the zero migration into the right-half-plane.

A second limitation in the effectiveness of DRFB flutter control is the saturation of the piezoelectric transducer. The applied control signal voltage is proportional to the strain rate and is therefore a function of the panel disturbance. In a realistic situation the disturbance would result from externally applied pressures such as turbulent boundary-layer (TBL) pressures. For simplicity in this investigation an initial displacement in the first mode of $r_1 = q_1/h_s = 1.0$ was used as the disturbance. The time history of the control signal was calculated for various Mach numbers and the dynamic pressure at which the maximum allowable piezoelectric voltage was reached was noted.

Results for transducer saturation are shown in Fig. 6. Note that for $M = 1.2$ the saturation curve corresponds with the potential flow flutter curve. Not until higher Mach numbers does the piezoelectric saturation significantly limit the ability to delay flutter onset. Considering piezoelectric saturation effects the flutter dynamic pressure is increased by 55% at $M = 1.2$, 28% at $M = 1.5$, and 26% at $M = 2.0$, as shown in Fig. 6.

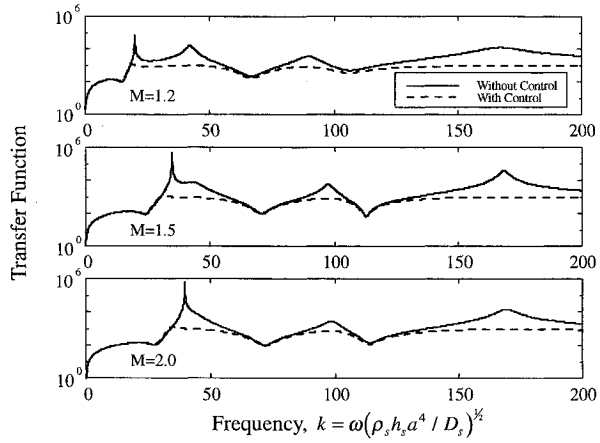

Fig. 10 Open- and closed-loop transfer functions.

Also note that while the application of collocated direct rate feedback control is effective for panel flutter control it is also effective for disturbance rejection. This is demonstrated in Fig. 10, which shows the open- and closed-loop transfer functions for three Mach numbers. In each case the dynamic pressure is just below the corresponding flutter dynamic pressure for that Mach number. The effect of direct rate feedback control in this case is to add damping to the near flutter poles, thus reducing the spectral peak.

Conclusions

The active control of panel flutter has been investigated including full linearized potential flow aerodynamic theory appropriate for the full transonic and supersonic Mach number range. Direct rate feedback control from a sensoriactuator piezoelectric transducer was modeled and its effectiveness in controlling flutter instability was demonstrated. It was shown that this type of control is capable of significantly increasing the flutter nondimensional dynamic pressure. It was also shown that this type of control is limited by the migration of the open-loop zeros into the right half-plane, thus, beyond a certain dynamic pressure, preventing the system from being stabilized. This zero migration to the right half-plane defines a new flutter boundary for the closed-loop aeroelastic panel. A second limitation was demonstrated in the saturation of the piezoelectric transducer.

Acknowledgments

This work was supported in part by the U.S. Air Force Office of Scientific Research, with Contract Monitor Jim Chang C.I.P.I., and the National Science Foundation Graduate Traineeship EE-92-56573.

References

[1]Scott, R. C., "Panel Flutter Suppression Using Adaptive Material Actuators," *Journal of Aircraft*, Vol. 31, No. 1, 1994, pp. 213–222.

[2]Hajela, P., "Application of Piezoelectric Elements in Supersonic Panel Flutter Suppression," AIAA Paper 91-3191, Sept. 1991.

[3]Hagood, N. W., Chung, W. H., and Von Flotow, A., "Modelling of Piezoelectric Actuator Dynamics for Active Structural Control," *Journal of Intelligent Material Systems and Structures*, Vol. 1, No. 3, 1990, pp. 327–354.

[4]Frampton, K. D., Clark, R. L., and Dowell, E. H., "State Space Modeling for Aeroelastic Panels Subject to Full Potential Flow Aerodynamic Loading," *Proceedings of the AIAA 36th Structures, Structural Dynamics, and Materials Conference* (New Orleans, LA), AIAA, Washington, DC, 1995, pp. 1183–1189.

[5]Dowell, E. H., "Generalized Aerodynamic Forces on a Flexible Plate Undergoing Transient Motion," *Quarterly of Applied Mathe-*

matics, Vol. 26, No. 3, 1967, pp. 2267–2270.

[6]Dowell, E. H., *Aeroelasticity of Plates and Shell,* Noordhoff International, Leyden, The Netherlands, 1975.

[7]Anderson, E. H., Hagood, N. W., and Goodliffe, J. M., "Self-Sensing Piezoelectric Actuation: Analysis and Application to Controlled Structures," *Proceedings of the AIAA 33rd Structures, Structural Dynamics, and Materials Conference* (Dallas, TX), AIAA, Washington, DC, 1992, pp. 2141–2155.

[8]Dosch, J. J., Inman, D. J., and Garcia, E., "A Self-Sensing Piezoelectric Actuator for Collocated Control," *Journal of Intelligent Material Systems and Structures*, Vol. 3, No. 1, 1992, pp. 166–185.

[9]Cole, D. G., and Clark, R. L., "Adaptive Compensation of Piezoelectric Sensoriactuators," *Journal of Intelligent Material Systems and Structures*, Vol. 5, No. 1, 1994, pp. 665–672.

[10]Evans, A. G., and Fischl, R., "Optimal Least Squares Time-Domain Synthesis of Recursive Digital Filters," *IEEE Transactions on Audio and Electroacoustics*, Vol. AU-21, No. 1, 1973, pp. 61–65.

[11]Marple, S. L., Jr., *Digital Spectral Analysis with Applications*, Prentice–Hall, Englewood Cliffs, NJ, 1987.

[12]Haykin, S., *Adaptive Filter Theory*, 2nd ed., Prentice–Hall, Englewood Cliffs, NJ, 1991.

[13]Hedgepeth, J. M., "Flutter of Rectangular Simply Supported Panels at High Supersonic Speeds," *Journal of the Aeronautical Sciences*, Vol. 24, No. 8, 1957, pp. 563–573.

[14]Johns, D. J., "A Panel Flutter Review," *Manual on Aeroelasticity*, Pt. III, AGARD, 1969, Chap. 7.

[15]Balas, M. J., "Direct Velocity Feedback Control of Large Space Structures," *Journal of Guidance, Control, and Dynamics*, Vol. 2, No. 3, 1979, pp. 252, 253.

[16]Vipperman, J. S., and Clark, R. L., "Hybrid Analog and Digital Adaptive Compensation of Piezoelectric Sensoriactuators," *Proceedings of the AIAA 36th Structures, Structural Dynamics, and Materials Conference* (New Orleans, LA), AIAA, Washington, DC, 1995, pp. 2854–2859.